

## Convective Instability and Structure Formation in Traffic Flow

Namiko MITARAI\* and Hiizu NAKANISHI\*\*

*Department of Physics, Kyushu University 33, Fukuoka 812-8581*

(Received April 21, 2000)

The effects of a localized perturbation in an initially uniform traffic flow are investigated with the optimal velocity model under an open boundary condition. The parameter region where the uniform solution is convectively unstable is determined by linear analysis. It is shown that the oscillatory flow, which is linearly unstable but convectively stabilized, is triggered out of a linearly unstable uniform flow by a localized perturbation, and in the upper stream it eventually breaks up into an alternating sequence of jams and free flows. This observation suggests that the real traffic flow pattern observed near an on-ramp [B. S. Kerner: Phys. Rev. Lett. **81** (1998) 3797] is a noise-sustained structure in an open flow system. We also find that, in a certain parameter region, the convectively stabilized uniform flow is destabilized by the non-linearly induced free flow.

KEYWORDS: traffic flow, synchronized flow, stop-and-go state, oscillatory flow, convective instability, pattern formation, noise-sustained structure, nonlinear absolute instability

### §1. Introduction

Everyone knows that a traffic flow on a freeway is not always smooth even when there is no obvious obstacle on the road. Based on serious field observations, it has been found out that there is a transition from the free flow to the jam at a certain density of cars;<sup>1)</sup> this is a major problem for traffic engineers because the transition reduces the car flux drastically and should be avoided. During the last several years, careful analysis of field data has revealed that there exist more dynamical states of flow other than the free flow and the jam; *the synchronized flow*<sup>2-5)</sup> is the flow where the velocity is lower than the free flow but the flux is relatively higher than the jam and the flow fluctuates synchronously between different lanes. *The stop-and-go state*<sup>4, 5)</sup> is the flow pattern where each car goes through an alternating sequence of jams and free flows in a short period of space and time. The synchronized flow is found in the high density region which could result in the jam, and often triggered by a localized perturbation such as an on-ramp; the stop-and-go state is often observed behind the synchronized flow region.<sup>4)</sup> The transition between the jam or the synchronized flow and the free flow has been observed and hysteretic behavior has been found.<sup>3, 4)</sup>

Physicists have been intrigued by the phenomenon because important roles must be played by fluctuations and instabilities, which are their old friends. Some managed to invent various kinds of phenomenological models that reproduce the free flow-jam transition appropriately.<sup>6-11)</sup> Then, the next target should be obviously to find out if these models are able to reproduce other flow states and patterns found in real traffic.<sup>12-19)</sup> In the simulations on macroscopic hydrodynamical traffic flow models with an on-ramp under the open boundary condition, vari-

ous kinds of dynamical states have been reported: For example, the oscillatory flows and the *convectively unstable* uniform flow are formed near the on-ramp,<sup>13, 14)</sup> and these flows are supposed to be the origin of the synchronized flow.<sup>13)</sup> However, the detailed features of these dynamical states such as stability against perturbation have not been clarified yet.

Such complex behaviors are also found in microscopic traffic flow models like car-following models<sup>16-18)</sup> and cellular automata (CA) models.<sup>19)</sup> The behavior of the optimal velocity (OV) model,<sup>7, 20)</sup> that is a one-dimensional car-following model, have been investigated under the periodic boundary condition, and found that the model is able not only to show the transition from the free flow to the jam, but also to reproduce the flux-density diagram (fundamental diagram).<sup>21)</sup> On the other hand, the present authors have investigated the OV model under an open boundary condition, and found that the oscillatory flow and the convectively unstable uniform flow realize in the OV model.<sup>17)</sup> Furthermore, it has been found that a localized perturbation triggers the spatio-temporal structure of the oscillatory flow followed by an alternating sequence of jams and free flows out of the uniform flow.<sup>18)</sup>

In this paper, we present detailed analysis on the effects of a localized perturbation in an initially uniform flow with the OV model under the open boundary condition.<sup>17, 18)</sup> The features of the convectively unstable uniform flow and the oscillatory flow are analyzed in detail, and it is shown that the structure formation in the OV model is understood as a pattern formation in a convectively unstable open flow system.<sup>22)</sup> We also show that the structure found in the real traffic can be interpreted as a *noise-sustained structure*, which is formed when small noise is added constantly to a convectively unstable uniform flow. It is also found that there is a parameter region where the structure is wiped away by a nonlinear effect, and that parameter region is deter-

\* E-mail: namiko@stat.phys.kyushu-u.ac.jp

\*\* E-mail: naka4scp@mbox.nc.kyushu-u.ac.jp

mined.

This paper is organized as follows. In §2, we introduce the OV model. In §3, the characteristic behaviors found in the numerical simulation are reported and analyzed in detail. Summary and discussion are given in §4.

## §2. The Optimal Velocity Model

In the OV model,<sup>7,20)</sup> the driver tends to drive at the optimal velocity determined by the headway of his car. When the  $(n+1)$ th car precedes the  $n$ th car, the position of the  $n$ th car  $x_n(t)$  at time  $t$ , obeys the equation of motion

$$\ddot{x}_n(t) = a[U(b_n(t)) - \dot{x}_n(t)], \quad (2.1)$$

with

$$b_n(t) = x_{n+1}(t) - x_n(t), \quad (2.2)$$

where the dots mean the time derivative and  $b_n(t)$  represents the headway of the  $n$ th car at time  $t$ . The parameter  $a$  is a sensitivity constant, and the function  $U(b)$ , called the OV function, determines the optimal velocity for a driver when his headway is  $b$ . From the physical consideration,  $U(b) \rightarrow 0$  as  $b \rightarrow 0$  and  $U(b) \rightarrow \text{const.}$  as  $b \rightarrow \infty$ . We employ

$$U(b) = \tanh(b-2) + \tanh(2), \quad (2.3)$$

as in most of works on the OV model.<sup>7,20,23)</sup>

Equation (2.1) has a uniform solution

$$x_n(t) = \bar{b}n + U(\bar{b})t, \quad (2.4)$$

which represents that all the cars go with the same headways  $\bar{b}$  and the same velocity  $U(\bar{b})$ . For later convenience, we briefly summarize the linear instability condition of the uniform solution.<sup>7,20)</sup> The linearized equation of motion around the uniform solution is given by

$$\Delta \ddot{x}_n(t) = a[U'(\bar{b})\Delta b_n(t) - \Delta \dot{x}_n(t)], \quad (2.5)$$

where the prime means the derivative by its argument, and  $\Delta x_n(t)$  and  $\Delta b_n(t)$  denote the deviation of the position and the headway, respectively. Assuming the form of its solution as

$$\Delta x_n(t) \propto \exp[i(kn - \omega t)], \quad (2.6)$$

we obtain

$$0 = (i\omega)^2 - a(i\omega) - aU'(\bar{b})(e^{ik} - 1) \equiv \Delta(\omega, k), \quad (2.7)$$

by which the dispersion relation in the “index frame” is determined. This equation has two solutions. The deviation from the uniform solution  $\Delta x_n(t)$  grows with time when  $\text{Im}[\omega_I(k)] > 0$ , where  $\omega_I$  is one of the solutions of eq. (2.7):

$$\omega_I(k) = -i\frac{a}{2} + \frac{i}{2}\sqrt{a^2 + 4aU'(\bar{b})(e^{ik} - 1)}. \quad (2.8)$$

The linear instability criterion is given by the condition  $\text{Im}[\omega_I(k)] > 0$  for any  $k$ , and the condition can be rewritten as

$$a < 2U'(\bar{b}). \quad (2.9)$$

When the linearly unstable uniform solution is per-

turbed under the periodic boundary condition, the effect of perturbation grows and eventually the system segregates into two regions; the jammed flow region with smaller headway and lower velocity, and the free flow region with larger headway and higher velocity.<sup>7,20,23)</sup> From the weak nonlinear analysis near the neutral stability line  $a = 2U'(\bar{b})$ , it has been shown that eq. (2.1) is reduced to the Korteweg-de Vries (KdV) equation when  $U''(\bar{b}) \neq 0$  ( $\bar{b} \neq 2$  when  $U(b)$  is given by eq. (2.3)), or to the modified KdV (MKdV) equation when  $U''(\bar{b}) = 0$  ( $\bar{b} = 2$ ).<sup>23)</sup>

## §3. Structure Formation in the OV Model

### 3.1 Three types of behavior-numerical results

We investigate the effect of a localized perturbation in an initial uniform flow in the situation where the upper and the lower stream is distinguished, which is more realistic for the freeway traffic flow than the periodic boundary condition. As we will see in the following, the difference in the boundary condition is crucial when one study the global structure formation.

In actual simulations, we set the boundary condition as follows: At the upper stream end ( $x = 0$ ), cars with the velocity  $U(\bar{b})$  enter the system with the constant time interval  $\bar{b}/U(\bar{b})$ . Around the lower stream end, the car that is farthest ahead, which has no car to follow within the system, obeys the equation of motion

$$\ddot{x}_{far} = a[U(\bar{b}) - \dot{x}_{far}], \quad (3.1)$$

and leaves the system at  $x = L$ . Here,  $\bar{b}$  is selected so that the uniform solution with the headway  $\bar{b}$  goes on when the initial condition is the uniform solution without perturbation.

Then we perturb the uniform solution locally in space and time by shifting the velocity of the 0th car at  $t = 0$  by a small value  $\epsilon$ , namely, we set the initial condition as

$$x_n(0) = \bar{b}n + L/2, \quad \dot{x}_n(0) = U(\bar{b}) \quad \text{for } n = \pm 1, \pm 2, \dots, \quad (3.2)$$

$$x_0(0) = L/2, \quad \dot{x}_0(0) = U(\bar{b}) + \epsilon. \quad (3.3)$$

In the numerical simulations, we found three qualitatively different regimes within the parameter region where the initial uniform solution is linearly unstable;<sup>17)</sup> The regime where the uniform solution is (i) linearly convectively unstable (Fig. 1(a)), (ii) linearly absolutely unstable (Fig. 1(b)), and (iii) absolutely unstable because of non-linear effect (Fig. 1(c)).

The instability is called *convective* if the perturbation grows with time but moves in space away from any fixed location in a given reference frame; the instability is called *absolute* if the perturbation grows with time at any point.<sup>24)</sup> This difference changes the global flow pattern significantly when the upper and the lower stream is distinguished, while it causes little change in the finite system under the periodic boundary condition where the growing perturbation never goes out of the system. Sufficient attention has not been paid to this difference in the analyses of the OV model under the periodic boundary condition.

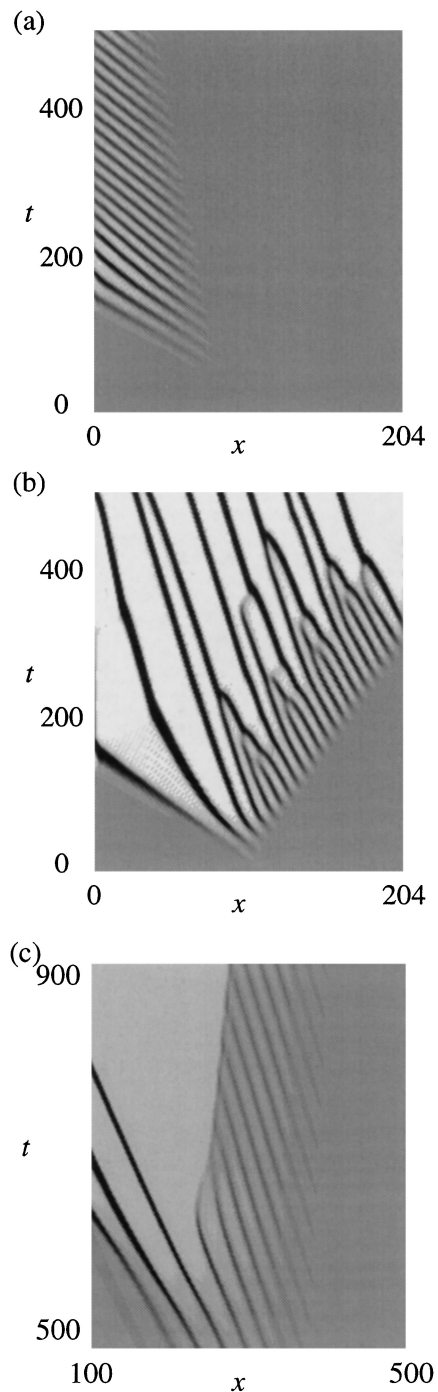


Fig. 1. The spatio-temporal diagrams of car density. The horizontal axis is the position of a car  $x$  and the vertical axis is time  $t$ . The higher density region is shown as a darker region. The darkness is adjusted so that the initial uniform flow region is shown by medium grey. (a)  $a = 1.4$ ,  $\bar{b} = 2.0$ ,  $\epsilon = 0.1$ ,  $L = 204$ . The uniform solution is linearly convectively unstable. (b)  $a = 1.0$ ,  $\bar{b} = 2.0$ ,  $\epsilon = 0.1$ ,  $L = 204$ . The uniform solution is linearly absolutely unstable. (c)  $a = 1.3$ ,  $\bar{b} = 2.5$ ,  $\epsilon = 0.1$ ,  $L = 800$ . The uniform solution is absolutely unstable because of nonlinear effect. The nonlinearly induced free flow region (the brighter region) invades the downstream oscillatory flow.

First we briefly review the behaviors in (i) and (ii). The uniform solution is linearly convectively unstable for the parameter  $a_c(\bar{b}) < a < 2U'(\bar{b})$ , where  $a_c(\bar{b})$  is the critical value that depends on  $\bar{b}$ . In this region, perturbation travels only upstream (Fig. 1(a)), therefore, the

disturbed region eventually goes out of the system, and the initial uniform solution is recovered. For  $a < a_c(\bar{b})$ , the system is in the linearly absolutely unstable region; the effect of the perturbation travels in both directions (Fig. 1(b)), and the uniform flow region is eliminated completely.

Except for the direction that the disturbance front travels, these two behaviors show a common spatio-temporal structure of flow if the system is large enough; The oscillatory flow region (a regular stripe pattern in Fig. 1(b)) is followed by an alternating sequence of jams and free flows (an irregular stripe with stronger contrast in Fig. 1(b)). In the oscillatory flow region, the headway and the velocity of cars oscillate periodically. This structure is spontaneously formed when the initial uniform solution is linearly unstable and the system size  $L$  is large enough; the structure persists until it goes out of the system.

On the other hand, the absolute instability caused by non-linear effect (iii) appears for relatively large value of  $\bar{b}$ . The initial time evolution is qualitatively the same as in the case of (i) or (ii). However, after the free flow region with lower car density is induced in the upper stream of the oscillatory flow region, the downstream edge of the free flow region advances and invades the oscillatory flow region (Fig. 1(c)). The oscillatory flow region is eliminated eventually, and the free flow region spreads over the whole system. Behind this free flow region, the short sequence of jams and free flows that is created by the initial perturbation remains.

In the rest of this section, we analyze these characteristic behaviors. In §3.2, we determine the parameter region in which the uniform solution is convectively unstable by the linear analysis. Then, we analyze the oscillatory flow in detail in §3.3. The spatio-temporal structure of flow in a large system is investigated in §3.4. The nonlinear absolute instability (iii) is discussed in §3.5.

### 3.2 Linear convective instability of uniform solutions

The difference between the convective instability and the absolute one depends on the reference frame.<sup>24)</sup> In the situation where the system has a specific boundary without Galilean invariance, the instability in *the laboratory frame*, which is stationary relative to the boundary, determines the system behavior. For simplicity, we first analyze the behavior observed in the index frame, which is moving with cars, following the procedure described in ref. 24, and then consider the behavior observed in the laboratory frame.

The nature of the instability can be determined by estimating the linear response to initially localized perturbation for large  $t$  at a fixed location.<sup>24)</sup> The solution of the linearized equation (2.5) for the initial state given by eqs. (3.2) and (3.3) may be written as

$$\Delta x_n(t) = \int_{-\infty+i\sigma}^{\infty+i\sigma} \frac{d\omega}{2\pi} e^{-i\omega t} \hat{x}(\omega, n), \quad (3.4)$$

$$\hat{x}(\omega, n) \equiv \int_{-\pi}^{\pi} \frac{dk}{2\pi} e^{ikn} \frac{\epsilon}{\Delta(\omega, k)}. \quad (3.5)$$

Where  $\sigma$  is a positive constant to define the integral

contour above which  $\hat{x}(\omega, n)$  is analytic. The function  $\Delta(\omega, k)$  has been defined in eq. (2.7). The asymptotic behavior of  $\Delta x_n(t)$  for large  $t$  at fixed  $n$  is determined by the pole of  $\hat{x}(\omega, n)$  in the  $\omega$  plane with the largest imaginary part; we denote such a pole as  $\omega = \omega_c$ . The pole  $\omega_c$ , in turn, is determined by the analytic structure of  $\Delta(\omega, k)$  in the  $k$ -plane as a function of  $\omega$ ;  $\omega_c$  is determined by the condition that the two zeros of  $\Delta(\omega, k)$  in the  $k$ -plane pinch the integral contour of eq. (3.5) when they merge into a double root. Therefore,  $\omega_c$  is given by

$$\left. \frac{d\omega_I(k)}{dk} \right|_{k=k_c} = 0, \quad \omega_I(k_c) = \omega_c, \quad (3.6)$$

and the asymptotic behavior of  $\Delta x_n(t)$  for large  $t$  is estimated as<sup>24)</sup>

$$\Delta x_n(t) \propto \frac{1}{\sqrt{t}} \exp[i(k_c n - \omega_c t)]. \quad (3.7)$$

The velocity with which the disturbance front propagates can be determined by considering the frame moving at the velocity  $V$  where the disturbance neither grows nor decays. The dispersion relation in the moving frame is given by

$$\omega_V(k) = -kV + \omega_I(k), \quad (3.8)$$

therefore, the condition corresponding to eq. (3.6) with  $\text{Im}[\omega_c] = 0$  in the moving frame becomes the equation

$$\left. \frac{d\omega_I(k)}{dk} \right|_{k=k_c} = V, \quad \text{Im}[\omega_I(k_c) - k_c V] = 0, \quad (3.9)$$

which is the marginal stability condition.<sup>25, 26)</sup> The first equation of eq. (3.9) has solutions  $k_{c+}$  and  $k_{c-}$ ;

$$k_{c\pm} = -i \text{Log}(z_{\pm}) + 2\pi m \quad (m = 0, \pm 1, \pm 2, \dots), \quad (3.10)$$

with

$$z_{\pm} = \frac{2V^2}{aU'(\bar{b})} \left[ 1 \pm \sqrt{1 + \frac{a}{4V^2}(a - 4U'(\bar{b}))} \right], \quad (3.11)$$

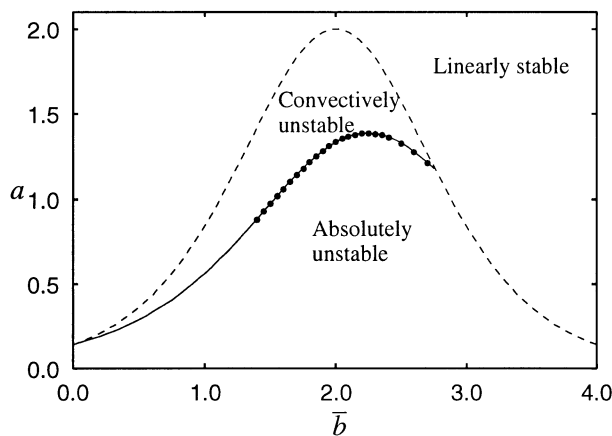


Fig. 2. The state diagram within the linear stability analysis. The solid line represents the boundary between convective instability and absolute instability  $a = a_c(\bar{b})$ . The linear neutral stability line  $a = 2U'(\bar{b})$  is also shown by the dashed line. The instability of the uniform solution is convective in the laboratory frame between the solid line and the dashed line. The filled circles are the parameter  $a = a_c(\bar{b})$  estimated by the numerical simulations.<sup>17)</sup>

where Log means the principal value of logarithm.  $k_c$  is the one out of  $k_{c\pm}$  which gives the larger imaginary value for  $\omega_V(k_{c\pm})$ ; the multivaluedness of the logarithm comes from the discreteness of the model and does not play any role in the analysis.

Our purpose is to determine the instability criterion in the laboratory frame, which is moving at the velocity  $-U(\bar{b})/\bar{b}$  relative to the index frame. This is given by eq. (3.9); the uniform solution is convectively (absolutely) unstable when  $V < -U(\bar{b})/\bar{b}$  ( $V > -U(\bar{b})/\bar{b}$ ). Solving eq. (3.9) numerically for  $a$  with  $V = -U(\bar{b})/\bar{b}$ , we obtain the boundary of the convective instability  $a = a_c(\bar{b})$ . In Fig. 2, the boundary  $a = a_c(\bar{b})$  is shown by the solid line. The dashed line represents the linear stability limit  $a = 2U'(\bar{b})$ . Between the solid line and the dashed line ( $a_c(\bar{b}) < a < 2U'(\bar{b})$ ), the uniform solution is convectively unstable in the laboratory frame, and the effect of localized perturbation is carried away from the system.

### 3.3 Oscillatory flow

Next we analyze the oscillatory flow, which appears as a regular stripe pattern in the spatio-temporal diagram of density (Fig. 1(b)). This can be observed more clearly in the snapshot of the headways of cars shown in Fig. 3. In Fig. 3(a), the linearly unstable uniform flow remains around the upper and the lower stream end of the system. Between the alternating sequence of jams and free flows (around  $-600 \lesssim n \lesssim -400$ ) and the uniform flow region in the lower stream ( $-310 \lesssim n$ ), we can see the region in which the headway of cars oscillates periodically. The amplitude of this oscillation is smaller than the difference between the upper and lower limiting values of headways in the alternating region. This oscillatory flow is spontaneously triggered out of the linearly unstable uniform flow by a localized perturbation and persists until the oscillatory flow region goes out of the system.

This oscillatory flow should be expressed by the solution in the form

$$b_n = \hat{b} + f(n - ct), \quad (3.12)$$

with the phase speed  $c$  and the periodic function  $f$ , which, we can assume, has zero average by taking  $\hat{b}$  as the mean headway; the value of  $c$  is negative since the stripe pattern propagates upstream.<sup>17)</sup> Substituting eq. (3.12) into eq. (2.1), we obtain

$$c^2 f''(z) = a[U(\hat{b} + f(z+1)) - U(\hat{b} + f(z)) + cf'(z)]. \quad (3.13)$$

with  $z \equiv n - ct$ . Equation (3.13) can be solved numerically in the minus direction of  $z$  axis when the initial condition for  $0 \leq z \leq 1$  is given. We integrated eq. (3.13) numerically with the initial condition that corresponds to the uniform solution with the headway  $h$  in the region  $0 < z \leq 1$  with small perturbation at  $z = 0$ :

$$f(z) = h - \hat{b}, \quad f'(z) = 0 \quad \text{for } 0 < z \leq 1 \quad (3.14)$$

and

$$f(0) = h - \hat{b} + \epsilon, \quad f'(0) = 0, \quad (3.15)$$

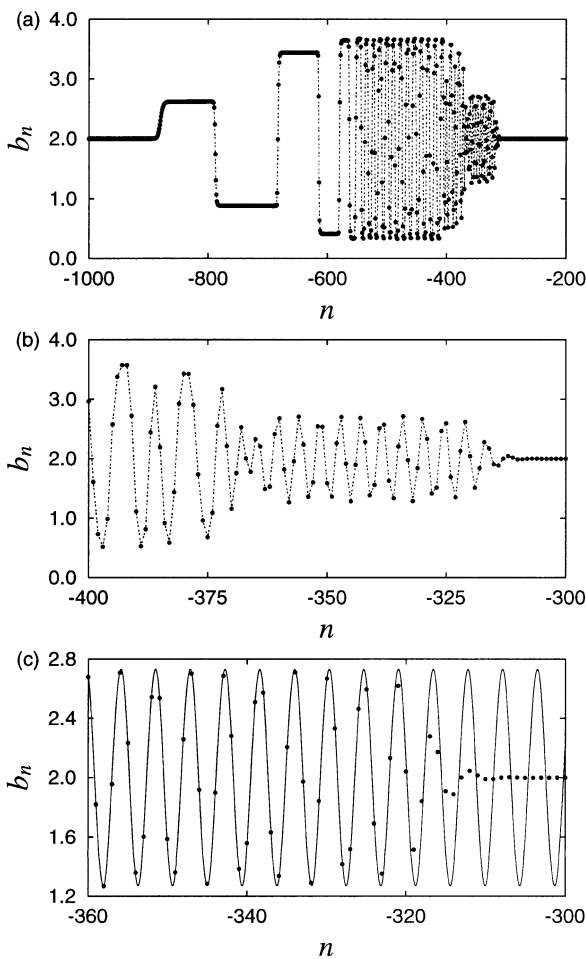


Fig. 3. The snapshots of the car configuration represented by the  $b_n$  vs  $n$  plot at  $t = 988$  with  $a = 1.0$ ,  $\bar{b} = 2.0$ ,  $\epsilon = 0.1$ , and  $L = 10000$  (the filled circles connected by the dashed line). (a) The oscillatory flow region appears around  $-360 < n < -310$  followed by the alternating sequence of jams and free flows which is found in  $-550 < n < -400$ . (b) The magnification of (a) around the oscillatory flow region. (c) The same data are plotted with the oscillatory solution (the solid line) from eq. (3.13) with  $a = 1.0$ ,  $h = 2.0$ ,  $c = c_{osc} = -0.610$ .

with  $\epsilon$  as small as  $10^{-10}$ . We found the oscillatory solutions for a finite range of the phase speed  $c$ ; e.g.,  $c \in (-0.637, -0.556)$  for  $a = 1.0$  and  $h = 2.0$ . When we set the phase velocity at the value obtained from the direct simulation of the original equation (2.1), namely,  $c = c_{osc} = -0.610$  for  $a = 1.0$  and  $\bar{b} = 2.0$ , we get  $f(n - c_{osc}t)$  which coincides with the result of the simulation,<sup>17)</sup> as is shown in Fig. 3(c).

It should be noted that the value  $h$  does not coincide with the mean headway  $\bar{b}$  except for the case of  $h = 2.0$ , around which the OV function is symmetric, namely  $[U(2 + \delta) - U(2)] = -[U(2 - \delta) - U(2)]$ . On the other hand, when  $h > 2$  ( $h < 2$ ),  $\bar{b}$  tends to be larger (smaller) than  $h$ , but  $\bar{b}$  depends on not only  $h$  but also  $a$  and  $c$ .

The shape of the oscillatory solution depends on  $a$ ,  $h$ , and  $c$ . When  $c$  approaches the lower limit of the allowed range in which the oscillatory solutions exist for given  $a$  and  $h$ , the amplitude and the wavelength become smaller, and the shape becomes sinusoidal (Figs. 4(a) and 4(b)). As  $c$  becomes larger ( $|c|$  becomes smaller), the am-

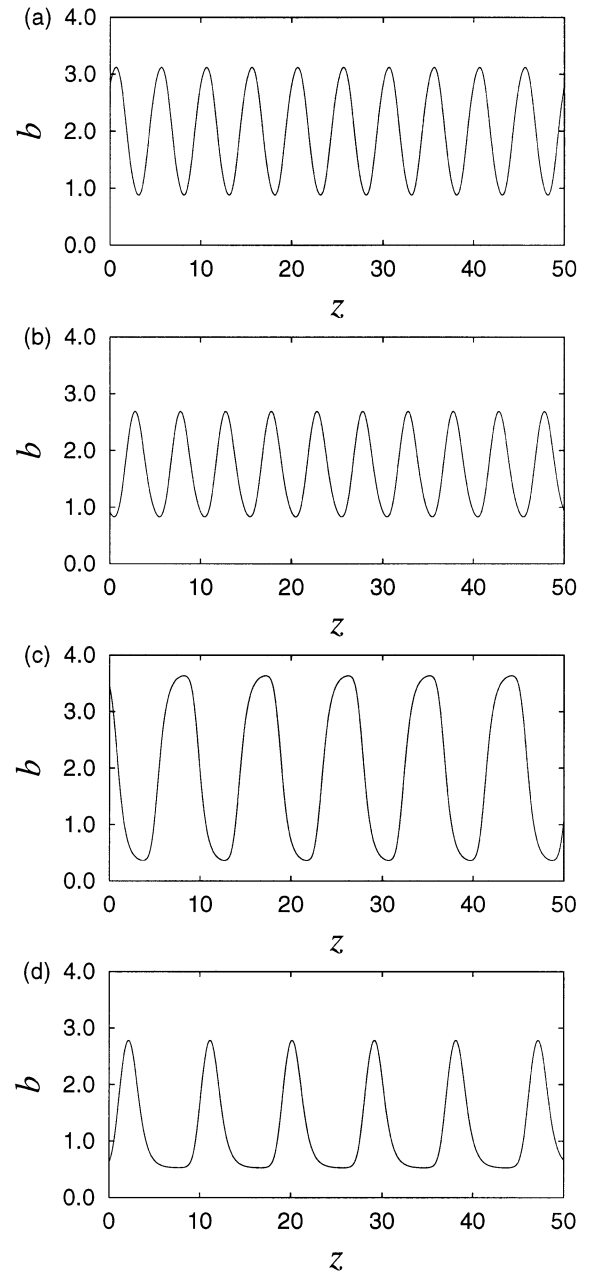


Fig. 4. The shape of the oscillatory solutions for various parameters. The value  $\lambda$  is the wavelength of the oscillatory solution measured in the index frame. (a)  $a = 1.0$ ,  $h = 2.0$ ,  $c = -0.584$ ,  $\lambda = 5.0$ . (b)  $a = 1.0$ ,  $h = 1.9$ ,  $c = -0.593$ ,  $\lambda = 5.0$ . (c)  $a = 1.0$ ,  $h = 2.0$ ,  $c = -0.557$ ,  $\lambda = 9.0$ . (d)  $a = 1.0$ ,  $h = 1.9$ ,  $c = -0.582$ ,  $\lambda = 9.0$ .

plitude and the wavelength become larger. When  $h = 2$ , the shape of the oscillatory solution looks like a sequence of pairs of kink and anti-kink (Fig. 4(c)), while it resembles a sequence of KdV solitons when  $h \neq 2$  (Fig. 4(d)). It is easy to show that, if  $f_0(z)$  is a solution of eq. (3.13) with  $\hat{b} = 2 - \delta$ , then  $-f_0(z)$  is also a solution of eq. (3.13) with  $\hat{b} = 2 + \delta$  because of the symmetry of  $U(b)$  at  $b = 2$ .

Now, we examine the linear stability of the oscillatory solutions by calculating the Floquet exponents, which can be regarded as the complex linear growth rate averaged over the period.<sup>27)</sup> When we calculate the Floquet exponents in the system with  $N$  cars, the headway of the  $(N + 1)$ th car is needed. We calculated the exponents

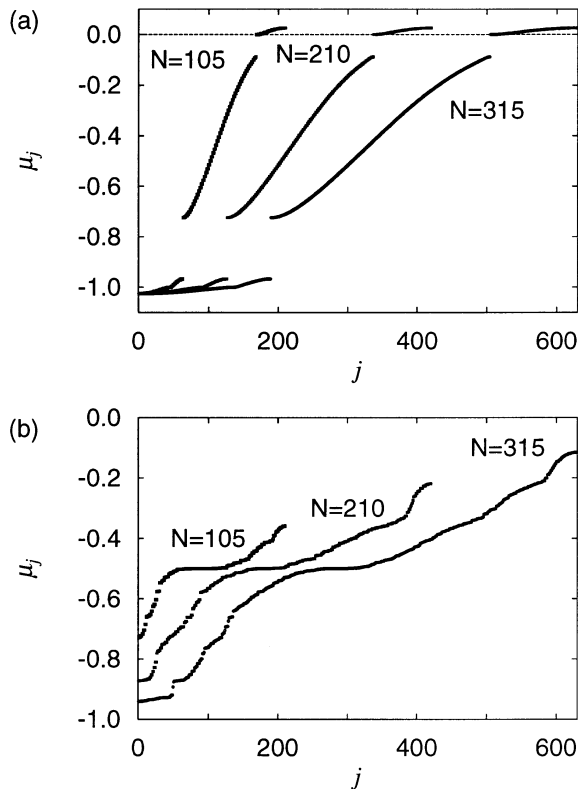


Fig. 5. The real parts of the Floquet exponents  $\mu_j$  for the oscillatory solution with  $a = 1.0$ ,  $h = 2.0$ ,  $c = -0.6837$  and  $\lambda = 5.0$ . The index of the exponents  $j$  is labeled so that the exponent with larger real part has a larger index. The value  $N$  in the figure indicates the number of cars in each calculations. (a) The value of  $\mu_j$  under the periodic boundary condition. Some of  $\mu_j$  are positive, which means the oscillatory solution is linearly unstable. (b) The value of  $\mu_j$  under the fixed boundary condition. All of  $\mu_j$  are negative, which means the oscillatory solution is linearly stable.

for the following two different boundary conditions: (i) The periodic boundary condition, where the headway of the  $(N + 1)$ th car equals to that of the first car. This boundary condition can be imposed only for the oscillatory solution whose wavelength measured in the index frame  $\lambda$  satisfies  $M\lambda = N$  with an integer  $M$ . (ii) The fixed boundary condition, where the oscillatory solution is imposed on the  $(N + 1)$ th car.

The real parts of the Floquet exponents  $\mu_j$  under each boundary condition are shown in Fig. 5. We can see that some of  $\mu_j$  are positive under the periodic boundary condition (Fig. 5(a)), while all of  $\mu_j$  under the fixed boundary condition are negative (Fig. 5(b)). This means the oscillatory solution is linearly unstable, but the growing perturbation is carried away if the headway of the foremost car obeys the oscillatory solution; namely, the linear instability of the oscillatory solutions is convective in the index frame.<sup>22)</sup>

The maximum value of real parts of the exponents under the periodic boundary condition  $\mu_{max}$  are listed in Table I for several values of  $\lambda$  and  $h$ . We can see that the value of  $\mu_{max}$  for the solution with  $h = 2$  tends to be smaller as the wavelength becomes longer. This tendency supports the conjecture by Komatsu and Sasa,<sup>23)</sup> who have performed the weak nonlinear analysis of the OV

Table I. The maximum real part of the Floquet exponent  $\mu_{max}$  for oscillatory solutions with  $a = 1.0$  calculated with  $N = 315$  under the periodic boundary condition. The value of  $\mu_{max}$  for the solution with  $h = 2.0$  tends to be smaller as  $\lambda$  becomes larger.

$\lambda$	$\mu_{max} (h = 2.0)$	$\mu_{max} (h = 1.9)$
4.2	0.0560	0.0576
4.5	0.0403	0.0427
5.0	0.0257	0.0315
7.0	0.0048	0.0402
9.0	0.0009	0.0388

model. They expected that the periodic solution of the MKdV equation becomes unstable because of the first-order correction term of the reduced equation, while the kink soliton, which can be regarded as a periodic solution with infinite wavelength, remains stable. We found, however, this is not a general tendency for the stability of the solution with  $h \neq 2$ .

### 3.4 Spatio-temporal structure of flow controlled by linear effect

In this subsection, we analyze the spatio-temporal structure of flow found in the simulations in the cases (i) and (ii). First we investigate how a particular oscillatory solution is selected in the situation described above, and then analyze the global spatial structure.

In these cases, the front propagation can be determined by the linear analysis in §3.2, and the front velocity  $V$  in the index frame and the complex wave number  $k_c$  in the linear regime are obtained from eq. (3.9) for a given set of  $a$  and  $\bar{b}$ . Then, the angular frequency  $\omega_c$  at the front in the frame moving with the front is given by

$$\omega_c = \omega_V(k_c) = -k_c V + \omega_I(k_c), \quad (3.16)$$

which is real due to eq. (3.9), and the phase velocity  $c_0$  in the index frame is

$$c_0 = \frac{\text{Re}[\omega_I(k_c)]}{\text{Re}[k_c]}. \quad (3.17)$$

These results are valid only in the linear regime.

Now, we conjecture that *the oscillatory frequency in the oscillatory flow, whose amplitude is in the nonlinear regime, is the same with that at front in the linear regime if they are observed in the moving frame with the front.* This is natural conjecture because the oscillatory flow is triggered by the oscillation at the front. We demonstrate that this is true by examining the frequency-wavelength relation in the moving frame

$$|\omega_c| = (V - c_{osc}) \frac{2\pi}{\lambda}, \quad (3.18)$$

where  $c_{osc}$  is the phase velocity of the oscillatory flow. In Table II, the two sets of data are listed: the one estimated from the linear analysis and the other estimated from the simulation data in the nonlinear region. The agreement is quite good.

However, this oscillatory solution cannot extend over the whole system, because it is only convectively stable as we have seen in §3.3. Instead, the motions of cars in the upper stream gradually deviate from the oscillatory

Table II. The data list which confirms the relationship in eq. (3.18). The values of  $c_0$  from eq. (3.17) and that from the simulation data are shown in order to check the linear analysis. The values of  $V_0$  and  $\omega_c$  are obtained from the linear analysis, and  $c_{osc}$  and  $\lambda$  are from the results of the simulations. The data show good agreement.

$a$	$\bar{b}$	$-c_0$	$-c_0$ (sim.)	$-V_0$	$-c_{osc}$	$\lambda$	$\frac{2\pi(V_0 - c_{osc})}{\lambda}$	$ \omega_c $
1.0	2.0	0.670	0.669	0.306	0.610	4.36	0.44	0.44
1.5	2.0	0.839	0.842	0.588	0.818	6.35	0.23	0.23
$2U'(\bar{b}) - 0.5$	1.8	0.799	0.804	0.552	0.781	6.28	0.23	0.23
$2U'(\bar{b}) - 1.0$	2.2	0.629	0.633	0.276	0.573	4.30	0.43	0.43
$2U'(\bar{b}) - 0.5$	2.2	0.799	0.806	0.552	0.781	6.28	0.23	0.23

solution, and eventually an alternating sequence of jams and free flows is formed.

Figure 6 shows the time evolution of the headway of the  $-578$ th car. If we see them from the bottom to the top, we can follow the patterns that the car goes through from the upper stream to the lower stream. In the following, however, we see them from the top to the bottom (from the lower to the upper stream), trying to understand the mechanism how the structure emerges out of the uniform flow. From the initial linearly unstable uniform flow in the lower stream, the small oscillation starts at the downstream front of the disturbed region (Fig. 6(a)). This oscillation grows as it travels upstream and the oscillatory flow region is formed when the amplitude saturates (Fig. 6(b)). This region breaks up in the upper stream because the oscillatory flow is stabilized only convectively (Fig. 6(c)), and the alternating sequence of jams and free flows is formed (Fig. 6(d)). This alternating region is not completely periodic, because any infinitesimal perturbation grows as it travels in the upstream direction. As a result, the spatio-temporal structure of the oscillatory flow region followed by the alternating region is observed.

This structure is always seen if the system is large enough, but the structure itself is moving in the system. When the instability of the uniform solution is convective, the structure eventually goes out of the system from the upper stream end. When the instability is absolute, the structure spreads in the system and is finally broken when the edge of the structure reaches to the boundary of the system. If small perturbation is added constantly to the convectively unstable uniform flow, however, the downstream front of the structure is fixed in space and the structure is sustained; such a structure is called a *noise-sustained structure* and often found in convectively unstable open flow systems, such as the complex Ginzburg-Landau equation with an advection term.<sup>22)</sup> Examples of the noise sustained structure, formed by adding small random noise to the velocity of the car when it passes the point  $x = x_b$ , are shown in Fig. 7. We can see that the structure appears and is pinned at  $x = x_b$  to extend to the upper stream. Once the convectively unstable uniform flow region is formed on a freeway, a noise-sustained structure should be observed, because stochastic noise is always present in the real traffic.

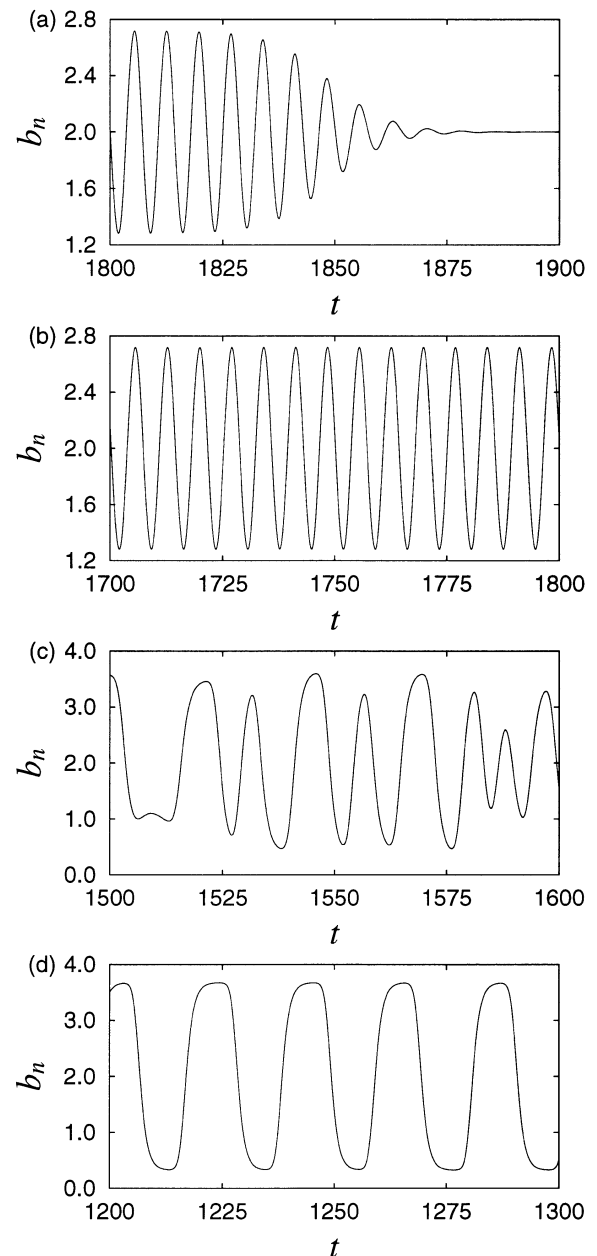


Fig. 6. The time evolution of the  $n = -578$ th car's headway  $b_n(t)$  with  $a = 1$ ,  $\bar{b} = 2$ ,  $\epsilon = 0.1$ , and  $L = 800$  (a) near the downstream front of the disturbed region where the oscillation starts, (b) within the oscillatory flow region where the amplitude of the oscillation saturates, (c) around the time where the oscillatory flow breaks up, and (d) in the alternating sequence of jammed and free-flow regions, which is not completely periodic.

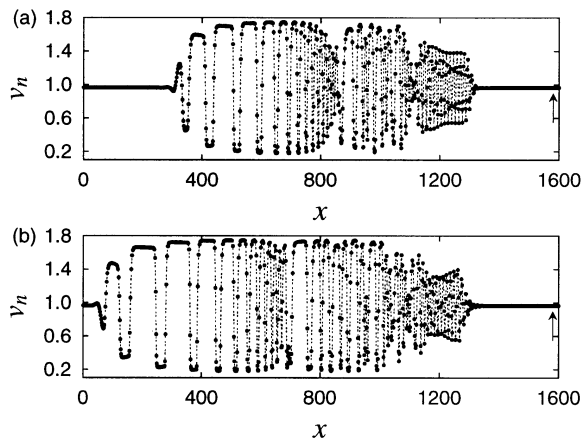


Fig. 7. The noise-sustained structure shown by the snapshots of the velocity. The horizontal axis is the position  $x$ , and the vertical axis is the velocity of cars  $v_n$ . The parameters are set so that the initial uniform solution is convectively unstable;  $a = 1.4$ ,  $\bar{b} = 2.0$ , and  $L = 1600$ . Every time a car passes the point  $x = x_b = 1580$  (indicated by an arrow), its velocity is shifted by random noise  $\epsilon_r$ , whose value is uniformly distributed between  $-5.0 \times 10^{-11}$  and  $+5 \times 10^{-11}$ . (a) The snapshot at  $t = 1556$ . (b) The snapshot at  $t = 1815$ .

### 3.5 Induced free flow by nonlinear effect

It is found in the simulations that the free flow region induced by perturbation in the upper stream invades the downstream oscillatory flow region when  $\bar{b}$  is relatively large (Fig. 1(c)). In this subsection, we estimate the parameter region in which this occurs.

In this case, the flow pattern is determined by the comparison with the velocity of the front of the oscillatory region in the laboratory frame  $V'$  and that of the free flow region  $V_{free}$ . The condition for the free flow region to invade the oscillatory flow region is given by

$$V_{free} > V'. \quad (3.19)$$

When this condition is satisfied, the spatio-temporal structure which we discussed in §3.4 is wiped away by the free flow; the oscillatory flow region is taken over and the uniform flow region is directly followed by the free flow region. Behind the free flow region, there remains the alternating region that is created by a perturbation. Especially the condition

$$V_{free} > 0 > V', \quad (3.20)$$

is important, because in this case the uniform flow region is eliminated in the laboratory frame even though its linear instability is convective, namely, *the instability is linearly convective but nonlinearly absolute*.<sup>26, 28)</sup>

We can calculate  $V'$  from

$$V' = \bar{b}V + U(\bar{b}), \quad (3.21)$$

where  $V$  is the velocity of the front of oscillatory flow in the index frame (defined in §3.4).

Now, we estimate the value of  $V_{free}$  in order to determine the stability limit by the inequalities (3.19) and (3.20). We can approximate the mean headway in the oscillatory flow region as  $\bar{b}$ , because the oscillatory flow region is smoothly connected to the uniform flow region.

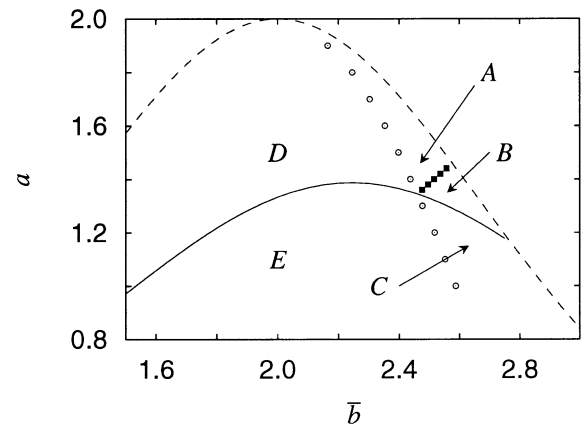


Fig. 8. The state diagram obtained from the linear and the nonlinear analysis. The parameter boundary of  $V_{free} = V'$  and  $V_{free} = 0$  are shown as open circles and filled boxes, respectively. The solid line is the boundary of  $V' = 0$  or  $a = a_c(\bar{b})$ , and the dashed line is the linear neutral stability line  $a = 2U'(\bar{b})$ . The oscillatory flow is invaded by the free flow in the regions A, B, and C. The region A:  $0 > V_{free} > V'$ , namely the instability of the uniform solution is nonlinearly convective. The region B:  $V_{free} > 0 > V'$ , namely the instability is linearly convective but nonlinearly absolute. The region C:  $V_{free} > V' > 0$ , namely the instability is nonlinearly absolute. The region D:  $0 > V' > V_{free}$ , namely the instability is linearly convective. The region E:  $V' > 0$  and  $V' > V_{free}$ , namely the instability is linearly absolute.

The headway in the free flow region  $b_{free}$  is almost constant, therefore  $V_{free}$  can be estimated as<sup>17)</sup>

$$V_{free} = -\frac{\bar{b}U(b_{free}) - b_{free}U(\bar{b})}{b_{free} - \bar{b}}, \quad (3.22)$$

from the condition of the continuity of the flux. The value of  $b_{free}$  depends on not only  $a$  and  $\bar{b}$  but also the amplitude of initial perturbation  $\epsilon$ . On the other hand, it has been shown numerically that the headway of the free flow region under the periodic boundary condition  $b_{fp}$  depends on  $a$  only.<sup>7, 20, 23)</sup> In the simulation, we found that the difference between  $b_{free}$  and  $b_{fp}$  is small, thus eq. (3.22) with

$$b_{free} = b_{fp}, \quad (3.23)$$

gives the good estimation of  $V_{free}$ , which depends on only  $a$  and  $\bar{b}$ .

The parameter boundary  $V_{free} = V'_0$  estimated by eqs. (3.21), (3.22), and (3.23) is shown in Fig. 8 by open circles, in which the boundary  $V_{free} = 0$  in the linearly convectively unstable region  $V'_0 < 0$  is also shown by filled boxes. In the regions A, B, and C, where  $V_{free} > V'_0$ , the oscillatory flow region is invaded by the free-flow region induced by the perturbation. The instability is nonlinearly absolute in the regions B and C: In the region B,  $V_{free} > 0 > V'_0$ , which means the initial uniform flow is eventually eliminated even though the linear instability is convective in the laboratory frame. On the other hand, in the regions D and E, the structure of flow which we have considered in §3.4 is maintained until the structure reaches to the boundary of the system.

#### §4. Summary and Discussion

In summary, we have examined the effects of a localized perturbation in an initially uniform traffic flow on the OV model in the system with an open boundary. The parameter region where the uniform solution is linearly convectively unstable in the laboratory frame has been determined. It has been also shown that the spatio-temporal structure of flow, the oscillatory flow followed by an alternating sequence of jams and free flows, is triggered out of the linearly unstable uniform flow by a localized perturbation. We have analyzed the oscillatory solutions in detail, and have found that they are linearly unstable but are convectively stabilized. It has been confirmed that the oscillatory flow that is triggered out of the uniform flow by a localized perturbation is linearly selected, and the mechanism of the global flow pattern formation can be understood in the general framework of the pattern formation in a convectively unstable open flow system. We also determined the parameter region where the oscillatory flow is invaded by non-linearly induced free flow and the convectively stabilized uniform solution within the linear regimes becomes absolutely unstable by the non-linearity.

In the following, we discuss the present results in connection with other traffic flow models and the real traffic flow observations.

First we consider car-following models including the OV model, in which each car never affected by the motion of the cars behind. As we have seen, the convective nature of instability in the index frame plays an important role in the structure formation. For the car-following models, it is evident that linearly unstable solutions are convectively unstable in the index frame, because a perturbation never affects preceding cars. On the other hand, analogous oscillatory behaviors have been also found in other car-following models.<sup>16, 29, 30)</sup> If these oscillatory flows are stabilized convectively, they could be triggered out of the unstable uniform flow and the structure formation mechanism examined in the present work should be common to such car-following models.<sup>31)</sup>

Another kind of traffic flow models is the CA model, in which the idea of linear instability does not exist. A phenomenon analogous to the convective stability, however, should be seen in the case where the car-car interaction is defined only through the distance to the preceding car.<sup>8, 10, 19)</sup> Therefore unstable flow can be convectively stabilized in the situation where the upper and the lower stream is distinguished. The oscillatory behavior is more difficult to realize in the CA models, in which all of the variables like velocity or position are treated as discrete ones. Recently, however, multi-value extension of CA models has been investigated, and some of the models have shown the complex behavior similar to the stop-and-go state.<sup>19)</sup> Therefore, the spatio-temporal structure may also be seen in such CA models as it is expected to be seen in car-following models.

In hydrodynamical models, we cannot follow the motion of each car, thus the nature of instability in the index frame is not clear. However, in the simulations under the open boundary condition with an on-ramp,<sup>13, 14)</sup>

convectively unstable uniform flow and oscillatory flows have been found to be triggered by influx of the on-ramp. It is not obvious if the oscillatory flows in the hydrodynamical models and that in the OV model have the same physical origin, because in the latter case we found that only a few cars are included in one wave length, therefore the validity of the continuous description is not apparent. Despite that, it is expected that a noise-sustained structure similar to the one found in the present work is seen in hydrodynamical models by adding small noise constantly to the convectively unstable uniform flow.

The spatio-temporal structure of flow is also observed in the real traffic flow;<sup>4)</sup> the synchronized flow followed by the stop-and-go state, which is often found near an on-ramp. This structure is analogous to the one found in the OV model, when we associate the oscillatory flow with the synchronized flow and the alternating region with the stop-and-go state. Based on this observation, we propose the following scenario to explain the structure formation in the real traffic: First, the convectively unstable uniform flow is formed by the influx from an on-ramp, as is seen in the hydrodynamical models.<sup>13, 14)</sup> Then, the oscillatory flow, which we believe is the synchronized flow, is triggered out of the convectively unstable uniform flow, due to the stochastic noise. The oscillatory flow is only convectively stabilized, therefore it breaks up in the upper stream. As a result, an alternating sequence of jams and free flows, namely the stop-and-go state, is formed in the upper stream of the oscillatory flow. This structure is maintained by the stochastic noise, namely, it is a noise-sustained structure.

Within the above scenario, the first step, i.e. the mechanism of the transition from the free flow to the convectively unstable uniform flow, is only speculation based on the corresponding simulations for hydrodynamical models. To clarify the condition where the linearly unstable uniform flow appears at least temporarily in the OV model is a future problem.

#### Acknowledgment

N. M. is grateful to K. Fujimoto for informative comments.

- 
- 1) B. S. Kerner and H. Rehborn: *Phys. Rev. E* **53** (1996) R1297.
  - 2) B. S. Kerner and H. Rehborn: *Phys. Rev. E* **53** (1996) R4275.
  - 3) B. S. Kerner and H. Rehborn: *Phys. Rev. Lett.* **79** (1997) 4030.
  - 4) B. S. Kerner: *Phys. Rev. Lett.* **81** (1998) 3797.
  - 5) L. Neubert, L. Santen, A. Schadschneider and M. Schreckenberg: *Phys. Rev. E* **60** (1999) 6480.
  - 6) B. S. Kerner and P. Konhäuser: *Phys. Rev. E* **48** (1993) R2335.
  - 7) M. Bando, K. Hasebe, A. Nakayama, A. Shibata and Y. Sugiyama: *Jpn. J. Ind. Appl. Math.* **11** (1994) 203.
  - 8) K. Nagel and M. Paczuski: *Phys. Rev. E* **51** (1995) 2909.
  - 9) S. Yukawa and M. Kikuchi: *J. Phys. Soc. Jpn.* **64** (1995) 35.
  - 10) K. Nagel: *Phys. Rev. E* **53** (1996) 4655.
  - 11) H. Hayakawa and K. Nakanishi: *Phys. Rev. E* **57** (1998) 3839.
  - 12) D. Helbing and M. Treiber: *Phys. Rev. Lett.* **81** (1998) 3042.
  - 13) D. Helbing, A. Hennecke and M. Treiber: *Phys. Rev. Lett.* **82** (1999) 4360.
  - 14) H. Y. Lee, H. W. Lee and D. Kim: *Phys. Rev. E* **59** (1999) 5101.

- 15) D. E. Wolf: *Physica A* **263** (1999) 438.
  - 16) E. Tomer, L. Safonov and S. Havlin: *Phys. Rev. Lett.* **84** (2000) 382.
  - 17) N. Mitarai and H. Nakanishi: *J. Phys. Soc. Jpn.* **68** (1999) 2475.
  - 18) N. Mitarai and H. Nakanishi: *Phys. Rev. Lett.* **85** (2000) 1766.
  - 19) K. Nishinari and D. Takahashi: preprint, nlin.AO/0002007.
  - 20) M. Bando, K. Hasebe, A. Nakayama, A. Shibata and Y. Sugiyama: *Phys. Rev. E* **51** (1995) 1035.
  - 21) M. Bando, K. Hasebe, K. Nakanishi, A. Nakayama, A. Shibata and Y. Sugiyama: *J. Phys. I (France)* **5** (1995) 1389.
  - 22) R. J. Deissler: *J. Stat. Phys.* **54** (1989) 1459.
  - 23) T. S. Komatsu and S. Sasa: *Phys. Rev. E* **52** (1995) 5574.
  - 24) E. M. Lifshitz and L. P. Pitaevskii: *Physical Kinetics* (Pergamon, Oxford, 1981) Chap. 6, p. 268.
  - 25) G. Dee and J. S. Langer: *Phys. Rev. Lett.* **50** (1983) 383.
  - 26) J. M. Chomaz and A. Couairon: *Phys. Rev. Lett.* **84** (2000) 1910.
  - 27) H. Haken: *Advanced synergetics: Instability hierarchies of self-organizing systems and devices* (Springer-Verlag, Berlin, 1983) Chap. 2, p. 89.
  - 28) A. Couairon and J. M. Chomaz: *Physica D* **108** (1997) 236.
  - 29) Y. Igarashi, K. Itoh and K. Nakanishi: *J. Phys. Soc. Jpn.* **68** (1999) 791.
  - 30) K. Nakanishi: *Phys. Rev. E* **62** (2000) 3349.
  - 31) The possibility of the formation of a noise-sustained structure in a car-following model has been already pointed out in ref. 22.
-